Preclinical activity of ABT-869, a multitargeted receptor tyrosine kinase inhibitor

Daniel H. Albert, Paul Tapang, Terrance J. Magoc, Lori J. Pease, David R. Reuter, Ru-Qi Wei, Junling Li, Jun Guo, Peter F. Bousquet, Nayereh S. Ghoreishi-Haack, Baole Wang, Gail T. Bukofzer, Yi-Chun Wang, Jason A. Stavropoulos, Kresna Hartandi, Amanda L. Niquette, Nirupama Soni, Eric F. Johnson, J. Owen McCall, Jennifer J. Bouska, Yanping Luo, Cherrie K. Donawho, Yujia Dai, Patrick A. Marcotte, Keith B. Glaser, Michael R. Michaelides, and Steven K. Davidsen

Cancer Research, Global Pharmaceutical Research and Development, Abbott Laboratories, Abbott Park, Illinois

Abstract

ABT-869 is a structurally novel, receptor tyrosine kinase (RTK) inhibitor that is a potent inhibitor of members of the vascular endothelial growth factor (VEGF) and platelet-derived growth factor (PDGF) receptor families (e.g., KDR IC_{50} = 4 nmol/L) but has much less activity (IC_{50}s > 1 μmol/L) against unrelated RTKs, soluble tyrosine kinases, or serine/threonine kinases. The inhibition profile of ABT-869 is evident in cellular assays of RTK phosphorylation (IC_{50} = 2, 4, and 7 nmol/L for PDGFR-β, KDR, and CSF-1R, respectively) and VEGF-stimulated proliferation (IC_{50} = 0.2 nmol/L for human endothelial cells). ABT-869 is not a general antiproliferative agent because, in most cancer cells, >1,000-fold higher concentrations of ABT-869 are required for inhibition of proliferation. However, ABT-869 exhibits potent antiproliferative and apoptotic effects on cancer cells whose proliferation is dependent on mutant kinases, such as FLT3. *In vivo* ABT-869 is effective orally in the mechanism-based murine models of VEGF-induced uterine edema (ED_{50} = 0.5 mg/kg) and corneal angiogenesis (>50% inhibition, 15 mg/kg). In tumor growth studies, ABT-869 exhibits efficacy in human fibrosarcoma and breast, colon, and small cell lung carcinoma xenograft models (ED_{50} = 1.5–5 mg/kg, twice daily) and is also effective (>50% inhibition) in orthotopic breast and glioma models. Reduction in tumor size and tumor regression was observed in epidermoid carcinoma and leukemia xenograft models, respectively. In combination, ABT-869 produced at least additive effects when given with cytotoxic therapies. Based on pharmacokinetic analysis from tumor growth studies, efficacy correlated more strongly with time over a threshold value (cellular KDR IC_{50} corrected for plasma protein binding = 0.08 μg/mL, ≥7 hours) than with plasma area under the curve or C_{max}. These results support clinical assessment of ABT-869 as a therapeutic agent for cancer. [Mol Cancer Ther 2006;5(4):995–1006]

Introduction

The reversible phosphorylation of proteins is one of the primary biochemical mechanisms mediating eukaryotic cell signaling. This reaction is catalyzed by protein kinases that transfer the γ-phosphate group of ATP to hydroxyl groups on target proteins (1). Five hundred eighteen such enzymes exist in the human genome, of which ~90 selectively catalyze the phosphorylation of tyrosine hydroxyl groups (2, 3). Cytosolic tyrosine kinases are intracellular, whereas receptor tyrosine kinases (RTK) possess both extracellular and intracellular domains and function as membrane spanning cell surface receptors. As such, RTKs mediate the cellular responses to environmental signals and facilitate a broad range of cellular processes, including proliferation, migration, and survival.

RTK signaling pathways are normally highly regulated. However, their overactivation has been shown to promote the growth, survival, and metastasis of cancer cells (4). In particular, members of the vascular endothelial growth factor (VEGF) and platelet-derived growth factor (PDGF) receptor families of RTKs promote tumor progression through a variety of mechanisms. VEGF RTKs KDR, FLT1, and FLT4 (VEGFR-2, VEGFR-1, and VEGFR-3) contribute to tumor progression through their ability to mediate tumor angiogenesis and lymphangiogenesis and to enhance vascular permeability. Results from clinical studies with Avastin have recently validated inhibition of VEGF signaling as a cancer target (5). RTKs from the PDGF family (PDGF-α, PDGF-β, FLT3, KIT, and CSF-1R) play a role in tumor angiogenesis and modify the tumor microenvironment in a fashion beneficial to tumor cell growth and metastasis. Additionally, mutations of FLT3 and KIT that result in constitutive kinase activity are directly associated with the proliferation of acute myeloid leukemia (AML) blast cells and gastrointestinal stromal tumor cells, respectively (6–13).

Although VEGF and PDGF RTKs are compelling cancer targets in and of themselves, preclinical studies indicate that greater antiangiogenic activity can be achieved by

Received 10/7/05; revised 1/30/06; accepted 2/21/06.

The costs of publication of this article were defrayed in part by the payment of page charges. This article must therefore be hereby marked advertisement in accordance with 18 U.S.C. Section 1734 solely to indicate this fact.

Requests for reprints: Daniel H. Albert, Cancer Research, Global Pharmaceutical Research and Development, Abbott Laboratories, R47J, Building AP9/2, 100 Abbott Park Road, Abbott Park, IL 60064-3500. Phone: 847-937-3844; Fax: 847-935-3622. E-mail: daniel.h.albert@abbott.com

doi:10.1158/1535-7163.MCT-05-0410

targeting these mechanisms simultaneously. Tumors are capable of secreting multiple angiogenic factors, and they depend on these factors at different stages of progression (14–20). For example, VEGF causes a large increase in blood vessel formation; yet, these vessels are immature and leaky. The formation of thicker, more stable vessels requires encapsulation by pericytes that is driven by PDGFR-β signaling (21, 22). Pericyte coverage is impaired by PDGFR-β inhibition, and microvessels lacking pericyte coverage regress upon deprivation of VEGF signaling (23, 24). Synergistic antiangiogenic effects may, therefore, be possible by targeting not only endothelial cells but also the supporting perivascular cells (24, 25).

The observation that the tumor microenvironment actively participates in tumor progression provides another reason to pursue agents capable of blocking multiple VEGF and PDGF receptor family members (26–28). Tumor-associated fibroblasts that express PDGFR-β are functionally distinct from normal fibroblasts and are thought to foster tumor cell invasion and metastasis through the release of growth factors and proteases (29). FLT1 and CSF-1R regulate the production and activation of tumor-associated macrophages that hasten the breakdown of the extracellular matrix by triggering gelatinase A expression (30, 31). KIT-expressing inflammatory mast cells have been implicated as accessory cells in tumor angiogenesis (32, 33). Simultaneous inhibition of these RTKs may, therefore, make the tumor microenvironment less hospitable for tumor growth. In addition, multitargeted VEGF/PDGF RTK inhibitors can also directly inhibit cancer cells whose proliferation is reliant on a mutant or overexpressed kinase, such as mutations in FLT3 observed in AML patients and KIT receptors in gastrointestinal stromal tumor and mast cell tumors (34–38).

The compelling nature of RTKs as anticancer targets provided the impetus for a search for potent and novel RTK inhibitors. The culmination of this search, ABT-869, is a novel multitargeted inhibitor of VEGF and PDGF receptor family members (Fig. 1). The present communication describes the *in vitro* and *in vivo* properties of ABT-869 in a preclinical setting that support future clinical studies in cancer therapy.

Materials and Methods

Compounds Used for Comparison Studies

The chemical structures and synthesis of the kinase inhibitors *N*-[4-(3-amino-1*H*-indazol-4-yl)phenyl]-*N*1-(2-fluoro-5-methylphenyl) urea (ABT-869; ref. 39), 6-[2-(methylcarbamoyl)phenylsulfanyl]-3-*E*-[2-(pyridin-2-yl)ethenyl]indazole (AG013736; ref. 40), 4-amino-5-fluoro-3-[6-(4-methyl-1-piperazinyl)-1*H*-benzimidazol-2-yl]-2(1*H*)-quinolinone (CHIR258; ref. 41), *N*-(3-trifluoromethyl-4-chlorophenyl)-*N*′-(4-(2-methylcarbamoyl-pyridin-4-yl)oxyphenyl)urea (BAY 43-9006; ref. 42), 5-[5-fluoro-2-oxo-1,2-dihydroindol-(3*Z*)-ylidenemethyl]-2,4-dimethyl-1*H*-pyrrole-3-carboxylic acid-(2-DEAE)amide (SU11248; ref. 43), and 1-(4-chloroanilino)-4-(4-pyridylmethyl) (PTK787; ref. 44) have been reported. These chemical entities were synthesized at Abbott for comparison studies and are designated in this article using the abbreviations previously used for these compounds.

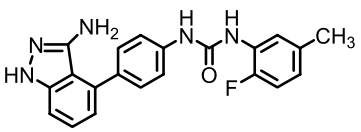

Figure 1. Structure of ABT-869: *N*-[4-(3-amino-1*H*-indazol-4-yl)phenyl]-*N*1-(2-fluoro-5-methylphenyl) urea. Molecular weight: 375.4 g/mol.

Kinase Assays

Potencies (IC_{50} values) were determined by assays of active kinase domains cloned and expressed in baculovirus using the FastBac baculovirus expression system (Life Technologies, Gaithersburg, MD) or obtained commercially. For tyrosine kinase assays, a biotinylated peptide substrate containing a single tyrosine was used with 1 mmol/L ATP, an Eu-cryptate–labeled anti-phosphotyrosine antibody (PT66), and Strepavidin-APC in a homogeneous time-resolved fluorescence assay (45). Serine/threonine kinases were assayed using 5 μmol/L ATP, [^{33}P]ATP, and a biotinylated peptide substrate with peptide capture and incorporation of ^{33}P determined using a SA-Flashplate (Perkin-Elmer, Boston, MA; ref. 46). Each inhibitor was assayed at multiple concentrations prepared by serial dilution of a DMSO stock solution of the compound. The concentration resulting in 50% inhibition of activity was calculated using nonlinear regression analysis of the concentration response data.

Receptor Phosphorylation

An ELISA-based screen in 3T3 murine fibroblasts engineered to express human KDR was used to evaluate KDR receptor phosphorylation and is described in detail elsewhere (47). A stimulatory autocrine loop in an angiopoietin-expressing 3T3 fibroblast line engineered to express human TIE2 was used to quantify inhibition of TIE2, and NIH3T3 cells engineered to express a KDR:KIT chimera (KDR extracellular domain fused to KIT transmembrane and intracellular domains) were used to quantify inhibition of KIT. In brief, autocrine or stimulated (50 ng/mL $VEGF_{165}$, R&D Systems, Minneapolis, MN) cells were incubated with inhibitor for 20 minutes. Lysates were prepared and added to plates precoated with capture antibody (receptor specific, coated into 96-well plates overnight followed by blocking with 3% nonfat milk in PBS) and incubated for 2 hours. Phosphorylated receptor was detected using anti-phosphotyrosine 4G10-biotin (UBI, Charlottesville, VA) and streptavidin-horseradish peroxidase (HRP; UBI). The HRP reaction was initiated with K-Blue substrate (Neogene Corp., Lexington, KY), quenched with 1 mol/L phosphoric acid and measured at 450 nm on a SpectraMax plate reader. For CSF-1R phosphorylation, NIH3T3 cells engineered to express human CSF-1R were stimulated for 10 minutes with M-CSF (200 ng/mL), lysed, and processed for Western blot by immunoprecipitation with anti-CSF1R antibody (Calbiochem, La Jolla, CA) with

detection after SDS-PAGE using anti-phosphotyrosine 4G10 and anti-mouse-HRP antibody. For PDGFR-β, lysates from PDGF-BB stimulated NIH3T3 cells (50 ng/mL for 5 minutes) were immunoprecipitated with anti-PDGFR-β antibody (SC-432, Santa Cruz Biotechnology, Santa Cruz, CA). Phosphorylated PDGFR-β was detected after SDS-PAGE with anti-phosphotyrosine 4G10-HRP 16-105, (Upstate Biotechnology, Charlottesville, VA). For KDR phosphorylation in cell lysates obtained from human umbilical artery endothelial cells (HUAEC; Cambrex Corp., East Rutherford, NJ), tumors, or lungs, the KDR antigen was concentrated by immunoprecipitation using an anti-VEGFR2 antibody (SC-6251, Santa Cruz Biotechnology or AF-357, R&D Systems). Phosphorylated KDR was visualized on Western blots using anti-phosphotyrosine 4G10-HRP (07-374, Upstate) and total KDR with anti-Flk-1 antibodies (SC-315 or SC-6251, Santa Cruz Biotechnology). Antigens were visualized by enhanced chemiluminescence with the Pierce Dura SuperSignal substrate (Pierce, Rockford, IL). The phosphotyrosine and total receptor bands were digitized by UN-SCAN-IT software (Silk Scientific, Orem, UT) for quantification. The anti-phosphotyrosine bands were normalized using the total receptor bands, and the percent inhibition was calculated at each concentration of inhibitor.

Cell Proliferation

HUAEC were plated into 96-well plates at 2,500 per well and incubated with serum-free medium for 24 hours. Drug and VEGF (final, 10 ng/mL) were added and incubated for 72 hours in serum-free medium. For carcinoma cell lines, 2,500 per well were plated overnight in full growth medium. Drug was added to the cells in full growth medium and incubated for 72 hours. For leukemia cells, generally 50,000 per well were plated in full growth medium, drug added, and incubated for 72 hours. The effects on proliferation were determined by addition of Alamar Blue (final solution, 10%), incubation for 4 hours at 37°C in a CO_2 incubator, and analysis in a fluorescence plate reader (544 nm, excitation: 590 nm, emission). For VEGF-stimulated growth, percent inhibition of proliferation was determined using the difference between VEGF-stimulated cells and unstimulated cells as the control, and IC_{50} values were determined by nonlinear regression analysis of the concentration response data.

Cell Cycle Analysis

Seventy-two-hour drug and vehicle-treated MV4-11 cells were fixed with 80% ethanol, washed with PBS, and then incubated with propidium iodide (50 μg/mL). DNA content was determined by fluorescence cell analysis using a FACSCalibur (BD Biosciences, San Jose, CA) flow cytometer, and cell cycle distribution was analyzed with CellQuest software. Apoptotic population (sub-G_0-G_1) was confirmed by Annexin V staining using the Annexin V-FITC Apoptosis Detection kit (BD PharMingen, San Diego, CA) according to the supplier's instructions.

Uterine Edema

Estradiol-induced edema in mice was measured following a procedure originally described in rat (48). Female BALB/c mice >12 weeks old were treated with 10 units of pregnant mare's serum gonadotropin at 72 and 24 hours before compound administration (0.1 mL/mouse i.p.). ABT-869 was orally given (n = 6) at various times before a 0.1 mL/mouse i.p. injection of 5 mg/mL 17β-estradiol. Mice were sacrificed 3 hours after estradiol injection. Uteri were removed, cleaned of fat and connective tissue, and weighed. Mean increase in weight above sham controls was computed and used to calculate percent inhibition of vehicle-treated control.

Corneal Angiogenesis

A hydron-sucralfate pellet, containing either 30 ng of basic fibroblast growth factor (bFGF; right cornea) or 150 ng VEGF (left cornea), was inserted into a corneal pocket made by surgical incision ~0.7 mm from the limbus of eyes of CF1 mice (Charles River Labs, Wilmington, MA). On day 5 (right cornea with bFGF) and again on day 7 (left cornea with VEGF pellet), a magnified corneal image was obtained by using a digital camera attached to a slit lamp biomicroscope. Data acquisition and storage were achieved with Leica imaging software. Statistical significance was evaluated with a two-tailed t test.

Tissue KDR Phosphorylation

VEGF-induced KDR phosphorylation in lung was assessed essentially as described (49). ABT-869 or vehicle was given by oral gavage to mice (three per group). At 1 or 3.5 hours after dosing, 3 μg VEGF was given via tail vein, and the animals were sacrificed 2 minutes later. Lungs were quickly resected and stored in liquid nitrogen until processed. Frozen tissue (175 mg/mL) was homogenized (PowerGen 35, Fisher Scientific, Pittsburgh, PA) for 30 seconds in radioimmunoprecipitation assay buffer [50 mmol/L Tris-HCl (pH 7.4), 1% IGEPAL, 150 mmol/L NaCl, 1 mmol/L EDTA, and 0.25% sodium deoxycholate] containing protease inhibitors (Complete, Roche Diagnostics, Indianapolis, IN) and NaF (1 mmol/L). After 1 hour at 4°C, the were lysates cleared by centrifugation at 15,000 rpm in a refrigerated microcentrifuge for 15 minutes. The supernatants were stored at −20 C until analysis of KDR phosphorylation as described above by Western blot analysis.

To assess duration of inhibition, lungs from mice bearing an HT1080 tumor in the flank (~1 g) were harvested 1 to 6 hours after treatment with ABT-869 and homogenized in radioimmunoprecipitation assay buffer, and the resulting extract was assayed for phosphorylated KDR using the ELISA as described in Receptor Phosphorylation.

Tumor Models

Cell lines were obtained from the American Type Culture Collection (Manassas, VA). For flank tumor xenograft studies, cells were suspended in PBS, mixed with an equal volume of Matrigel (phenol red free; BD Biosciences), and inoculated into the flank of mice of the indicated strain. For orthotopic models, cells were inoculated into either the mammary fat pad (breast) of mice or intracranially (glioma) into the right cerebral hemisphere 3 mm in depth and 2.5 mm lateral, 2 mm anterior to the bregma in Fisher rats. The

number of cells inoculated were 0.2 million (H526, DLD-1, MDA-231, MDA-435LM, and HCT-116), 0.5 million (HT1080, A431, and 9L), and 7.5 million (MV4-11). MX-1 cells were inoculated as a 1:10 dilution of brei obtained from 0.25 g of tumor propagated in severe combined immunodeficient mice. At the designated time after inoculation, tumor-bearing animals were divided into groups ($n = 10$), and administration of vehicle (2% ethanol, 5% Tween 80, 20% PEG400, 73% saline) or inhibitor at the indicted dose was initiated. Tumor growth in the flank was assessed by measuring tumor size with calipers and calculating size using the formula ($L \times W^2/2$). Tumor volume for the orthotopic glioma model was determined using magnetic resonance imaging. Inhibition of solid tumor growth on a specific day or tumor size was represented as mean volume of the test drug group over the mean volume of the untreated (control) group (T/C) or as percent inhibition of control [$(1 - T/C) \times 100$].

Immunohistochemistry

Mice with established MDA-231 tumors (0.2–0.3 g) were given ABT-869 (12.5 mg/kg, twice daily or bid) or vehicle for 3.5 days. Tumors were harvested 4 hours after final treatment, fixed in Streck Tissue Fixative, and paraffin embedded. Five-micrometer sections were incubated with monoclonal rat anti-mouse CD31 antibody (BD PharMingen) followed by biotinylated rabbit anti-rat immunoglobulins (DAKO, Carpinteria, CA), then by StreptABC complex/HRP (DAKO). Mosaic pictures of whole tissue section stained for CD31 were taken with Zeiss Axioplan2 Image Microscope. The density of microvessels outlined by CD31-positive endothelial cells in tumors was analyzed with AxioVision4.1 image measuring and analyzing program (Carl Zeiss MicroImaging, Inc., Thornwood, NY).

Drug Plasma Exposure

At the terminus of tumor growth studies, each test group ($n = 10$) was dosed with drug, and blood was withdrawn over a 12-hour period. Plasma (100 μL) obtained from the blood samples was diluted with 1 volume of 10% methanol, 25 μL of 0.25 mmol/L Na_2CO_3 and extracted twice with 3 volumes of ethyl acetate. After removing the ethyl acetate under nitrogen, the residue was reconstituted in methanol and subjected to high-performance liquid chromatography using UV detection (225 nm) on a YMC ODS-A column (Waters Corp., Milford, MA) eluted with acetonitrile/10 mmol/L sodium acetate (pH 5.5; 43:57, v/v). The detection limit for ABT-869 was ~20 nmol/L with an extraction efficiency of 68%.

Results

Intrinsic Potency and Selectivity of ABT-869

The potency of ABT-869 for inhibiting targeted RTKs is given in Table 1. For comparison, potency against a set of nonrelated RTKs and serine/threonine kinases is also provided. ABT-869 exhibits IC_{50} values that range from 4 nmol/L (KDR) to 190 nmol/L (FLT4) for members of the VEGF and PDGF receptor families. The molecule is also active against TIE2 and, to a lesser extent, RET, but is much less active ($IC_{50} > 10$ μmol/L) against other nonrelated tyrosine kinases, such as steroid receptor coactivator and epidermal growth factor receptor. ABT-869 was also generally not effective against serine/threonine kinases. Of those evaluated, only SGK was significantly inhibited at concentrations of ABT-869 below 1 μmol/L ($IC_{50} = 0.94$ μmol/L). This activity was measured at low ATP (5 μmol/L compared with 1 mmol/L for tyrosine kinase assays). Because ABT-869 has been shown to be an ATP-binding site competitive inhibitor (47), any activity against serine/threonine kinases observed in these studies is most likely an overestimation of activity that would be observed in the high-ATP cellular environment. As is discussed later (see Comparison to Other Tyrosine Kinase Inhibitors), this pattern of selectivity toward VEGF and PDGF RTK families remains evident after assessment against a broader range of kinases.

Cellular Activity of ABT-869

The potency of ABT-869 against tyrosine kinase enzyme preparations is reflected in receptor-mediated responses to

Table 1. Kinase inhibition profile of ABT-869

Related RTK*		Nonrelated TK*		Serine/threonine kinases †	
Kinase	IC_{50} (nmol/L)	Kinase	IC_{50} (nmol/L)	Kinase	IC_{50} (nmol/L)
KDR	4	SRC	>50,000	AKT	>50,000
FLT1	3	IGFR	>50,000	SGK	940
FLT4	190	INSR	>50,000	CDC2	9,800
PDGFRβ	66	LCK	38,000	PKA	5,900
CSF-1R	3	EGFR	>50,000		
KIT	14	HCK	>50,000		
FLT3	4	CMET	>50,000		
TIE2	170	LYN	>20,000		
RET	1,900	FYN	>50,000		
FGFR	>12,500	FGR	>50,000		

*IC_{50}s determined at an ATP concentration of 1 mmol/L.
†IC_{50}s determined at an ATP concentration of 5 to 10 μmol/L.

Table 2. Activity of ABT-869 in cellular receptor phosphorylation assays

Cell	Receptor	Ligand	Protein*	IC_{50} (nmol/L)
HUAEC	KDR	VEGF	—	2
3T3 transfectants	KDR	VEGF		4
			Mouse plasma	240
			Human plasma	340
3T3 transfectants	PDGFR-β	PDGF-BB	—	2
3T3 transfectants	KIT	VEGF	—	31
3T3 transfectants	CSF-1R	CSF-1	—	10
3T3 transfectants	TIE2	Autoactivation	—	3,500

*50% mouse or human plasma.

VEGF and PDGF at the cellular level. Phosphorylation of KDR induced by VEGF was inhibited by ABT-869 with an IC_{50} of 4 nmol/L in 3T3 murine fibroblasts engineered to express human KDR. (Table 2). A similar potency for inhibition of receptor autophosphorylation was seen with ABT-869 when HUAECs were used as the target cell. Because of the low abundance of KDR in these cells, an ELISA format could not be used, and the analysis was done using immunoprecipitation and Western blot techniques. As shown in Fig. 2A, ABT-869 inhibited VEGF-stimulated phosphorylation of KDR completely at 10 nmol/L and by ~70% at 3 nmol/L (IC_{50} ~ 2 nmol/L). Taken together, these results clearly show that ABT-869 is a potent inhibitor of KDR phosphorylation in engineered cell lines and primary endothelial cells.

The enzyme-inhibitory activity of ABT-869 against other tyrosine kinases was also evident in cellular assays. ABT-869 showed significant activity against ligand-induced PDGFR-β, KIT, and CSF-1R phosphorylation, with IC_{50}s of 2, 31, and 10 nmol/L, respectively (Table 2). Indeed, in the case of PDGFR-β, ABT-869 was substantially more potent in the cellular assay than in the enzyme assay (2 versus 66 nmol/L). In contrast, cellular TIE2 autophosphorylation was less sensitive to ABT-869 than other family members and required a concentration of 3,500 nmol/L to reach 50% inhibition of receptor activity. The reasons for these discrepancies are not known, but they may reflect the artificiality of the isolated kinase assays (e.g., truncated kinase domains, synthetic substrates, and high ATP concentration). Consequently, cellular potency may be more predictive of *in vivo* activity.

Receptor phosphorylation in the VEGF pathway is an important mitogenic signal for endothelial cells (50). As expected, ABT-869 inhibited VEGF-stimulated HUAEC proliferation (Table 3), although the IC_{50} was 5- to 10-fold lower than would be predicted by activity in the cellular phosphorylation and enzyme inhibition assays. In contrast, with a panel of tumor cells grown in serum-containing media (Table 3), ABT-869 had only weak activity (IC_{50} > 1 μmol/L) against cells whose proliferation is not driven by a VEGF or PDGF tyrosine kinase, such as HT-29 and MDA-435 carcinoma cells. Antiproliferative effects in these cellular assays is observed at >1,000-fold higher ABT-869 concentrations than in the VEGF-stimulated HUAEC assay. ABT-869 did potently inhibit (IC_{50} = 4 nmol/L; Table 3) the proliferation of MV4-11 leukemia cells that are known to express a constitutively active form of FLT3 (FLT3-ITD; ref. 51).

It is worth noting that the cellular potency of ABT-869 is affected by serum protein. The presence of 50% mouse or human plasma increased the IC_{50} value for inhibiting KDR phosphorylation by a magnitude (60- and 85-fold; Table 2) that closely approximates the free fraction predicted by the protein binding of ABT-869 in serum (98.2% and 99.0%,

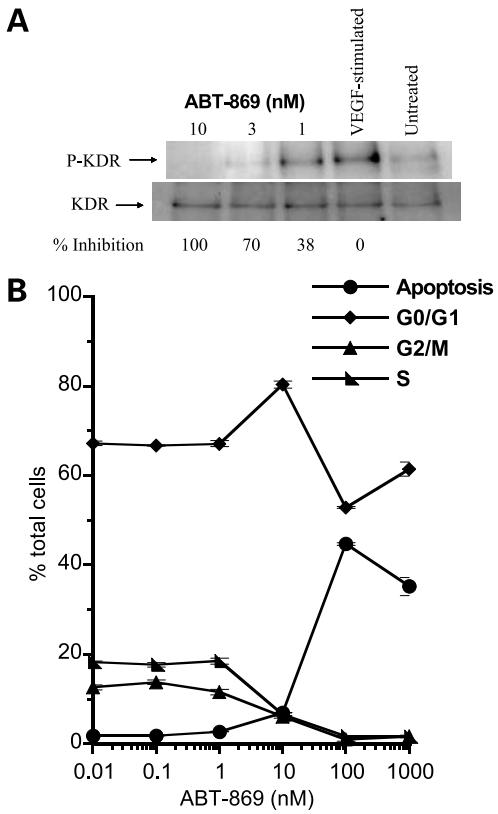

Figure 2. Inhibition of cellular responses with ABT-869. **A,** VEGF-stimulated KDR phosphorylation in HUAECs. Cells were exposed to 50 ng/mL VEGF and incubated with inhibitor for 20 min. **B,** cell cycle effects of ABT-869 on MV4-11 cells. Cells were incubated with ABT-869 at the indicated concentration for 72 h before cell cycle analysis.

Table 3. Inhibition of cell proliferation

Cell type	Source	Growth factor*	IC_{50} (nmol/L)
Endothelial	HUAEC	VEGF	0.2
Colon carcinoma	HT-29	FBS	1,300
Fibrosarcoma	HT1080	FBS	6,800
Epidermoid carcinoma	A431	FBS	3,200
Breast carcinoma	MDA-435	FBS	2,400
Breast carcinoma	MDA-231	FBS	>10,000
Small cell lung carcinoma	H526	FBS	4,500
Colon carcinoma	DLD-1	FBS	>10,000
Rat glioma	9L	FBS	270
AML (FLT3-ITD)	MV4-11	FBS	4.0

NOTE: Cells were incubated with ABT-869 for 72 hours.
*VEGF, 10 ng/mL; FBS, 10% fetal bovine serum.

respectively). These results suggest that potency determined in ''protein-free'' settings, such as those used to assess VEGF-stimulated HUAEC proliferation, may be shifted as much as 85 fold in the presence of physiologically relevant protein concentrations. Thus, the IC_{50} value for HUAEC proliferation could shift to as high as 20 nmol/L in the presence of serum, a concentration still well below that necessary to inhibit the proliferation of non–VEGF-dependent tumor cells (Table 3).

The antiproliferative effect of ABT-869 was associated with changes in the cell cycle profile and survival of MV4-11 cells evident after Annexin V/propidium iodide flow analysis. Exposure to ABT-869 for 72 hours caused a decrease in S and G_2-M phases with a corresponding increase in the sub-G_0-G_1 apoptotic population (Fig. 2B). An increase in apoptosis to a similar magnitude was also observed by measuring Annexin staining at 24 and 48 hours (7% and 12%; data not shown). The induction of apoptosis coupled with the antiproliferative effect of ABT-869 are in keeping with the strong survival signal provided by mutated FLT3 in AML (51).

Inhibition of VEGF-Mediated Responses *In vivo*

Murine lung expresses a high level of KDR and as such provides an accessible target organ to monitor the *in vivo* effects of receptor kinase inhibitors on ligand-mediated receptor activation (49). Inhibition of KDR phosphorylation was assessed using immunoprecipitation/Western blot techniques with lung tissue obtained from mice dosed with ABT-869 before administration of VEGF. As is shown in Fig. 3A, oral administration of ABT-869 resulted in inhibition of KDR phosphorylation in lung tissue. When assessed 1 hour after dosing, a dose of 0.3 mg/kg provided complete inhibition (Fig. 3A, *left*). When the sampling time was extended to 3.5 hours after dose, a period more reflective of the duration of significant inhibition observed in a VEGF response model after an efficacious dose of

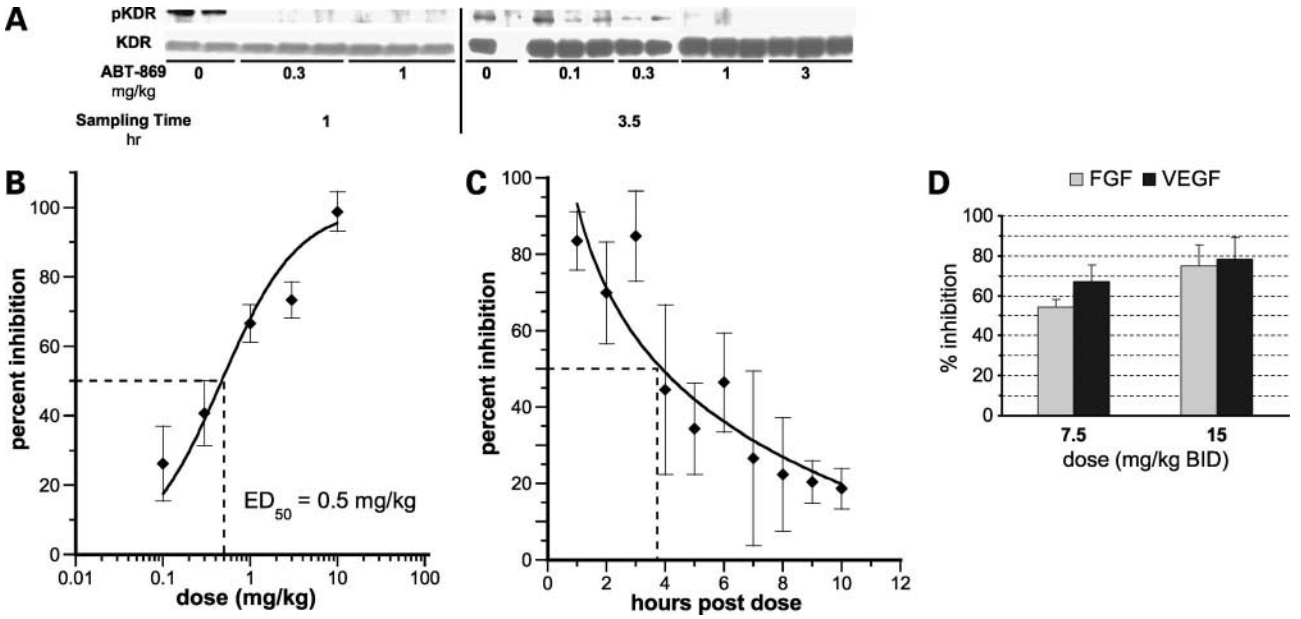

Figure 3. Inhibition of VEGF-mediated responses *in vivo*. **A,** VEGF-induced KDR phosphorylation. ABT-869 was administered (orally) at the indicated dose either 1 h (*left*) or 3.5 h (*right*) before i.v. challenge with VEGF (3 μg). **B,** VEGF-induced uterine edema. Mice (six per group) were given ABT-869 at the indicated dose (orally) and challenged with estradiol 30 min later. Edema was assessed 2 h after dosing. *Points,* mean percent inhibition; *bars,* SE. Mean uterine weights: control, 92 ± 7 μg; estradiol, 167 ± 3 μg. Values >30% were significantly different ($P < 0.05$) from control. **C,** duration of inhibition of uterine edema following administration of ABT-869. Mice were given ABT-869 (5 mg/kg, orally) and challenged with estradiol at the indicated times thereafter. Uterine edema was assessed as described in the text. Mean uterine weights: control, 94 ± 4 μg; estradiol, 152 ± 6 μg. Values >30% were significantly different ($P < 0.05$) from control. **D,** growth factor–induced murine cornea angiogenesis. *Columns,* mean inhibition ($n = 6$ per group); *bars,* SE. Control (vehicle) area (pixels): bFGF, 310,738 ± 20,383; VEGF, 334,653 ± 18,060. $P < 0.001$, compared with vehicle treated for each drug treatment group.

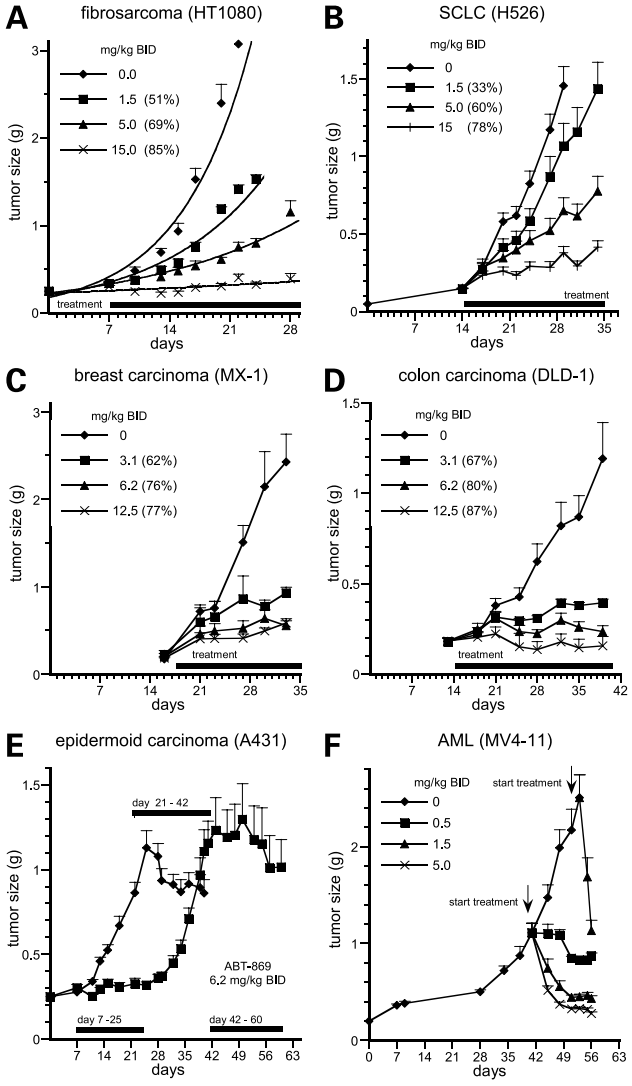

Figure 4. Activity in human xenograft models. Effects of ABT-869 on the growth of HT1080 (**A**), H526 (**B**), and MX-1 (**C**) human tumor cells implanted s.c. in the flank of severe combined immunodeficiency disorder and DLD-1 (**D**) cells implanted in nude mice. Oral dosing (bid) started on the day indicated by the solid bar along the *x* axis. *Points,* mean tumor volumes (n = 10 per group); *bars,* SE. Significant differences ($P < 0.05$ versus control) in mean tumor volume were observed for all treatment groups by the end of the study. Percent inhibition of control on day 21 (HT1080), day 28 (H526), day 33 (MX-1), and day 40 (DLD-1) in brackets. A431-derived (**E**) and MV4-11-derived (**F**) tumors. ABT-869 or vehicle was administered orally bid and continued as indicated.

ABT-869 (see below), a dose of 3 mg/kg was required for complete inhibition of receptor phosphorylation (Fig. 3A, *right*). These results show that ABT-869 inhibits ligand-induced phosphorylation of a target receptor, and that a dose level of at least 3 mg/kg is required for complete inhibition for >3.5 hours. Increased vascular permeability, a hallmark of VEGF-induced responses in the uterus, serves as an *in vivo* indication of ligand activation of KDR in surrogate tissue (48, 52). As shown in Fig. 3B, ABT-869 given orally inhibited the edema response in a dose-dependent manner with a potency (ED_{50} = 0.5 mg/kg) that agreed well with the potency for inhibiting receptor phosphorylation of ABT-869 in lung. The acute response to estradiol challenge was also used to evaluate duration of inhibition of a VEGF-mediated response following a single dose of ABT-869. The dose chosen for these studies (5 mg/kg) is sufficient (when given bid) to produce 60% to 70% inhibition in most of the tumor growth models discussed below. As shown in Fig. 3C, administration of this dose resulted in >50% inhibition of the VEGF response for 3 to 4 hours. This corresponds to an inhibition of VEGF-mediated responses for ~6 to 8 hours in a 24-hour period with the compound given bid.

ABT-869 was also effective in an *in vivo* model of growth factor–induced angiogenesis. When given daily for 5 days (bFGF) or 7 days (VEGF), ABT-869 (7.5 and 15 mg/kg bid) significantly ($P < 0.001$) inhibited both bFGF- and VEGF-induced increases in vessel density in the cornea (Fig. 3D). A similar pattern was observed when angiogenesis was quantified by vessel length (data not shown). The efficacy for inhibition of angiogenesis induced by VEGF is consistent with the potency for inhibiting KDR phosphorylation in lung. However, ABT-869, in spite of a lack of significant potency for inhibiting FGF receptor (Table 1), also inhibited bFGF-induced angiogenesis. This activity is most likely due to the role of VEGF and PDGF family member kinases in FGF signaling and has been reported for other small molecule inhibitors (53).

Activity in Human Xenograft Tumor Growth Models

ABT-869 has been evaluated in flank xenograft models using human tumor cell lines that represent a broad range of tumor types, including a highly angiogenic fibrosarcoma (HT1080; refs. 54, 55), a small cell lung carcinoma known to express KIT (H526; ref. 56), colon carcinoma (DLD-1), and breast carcinoma (MX-1; ref. 57). Treatment with ABT-869 inhibited tumor growth in each of these models in a dose-dependent manner (Fig. 4A-D), although the potency for robust inhibition (ED_{75}) varied from a low of 4.5 mg/kg bid (colon carcinoma) to a high of 12 mg/kg bid (small cell lung carcinoma). Within this group, the fibrosarcoma (7.5 mg/kg bid) and breast carcinoma (6 mg/kg bid) were intermediate in sensitivity to ABT-869 treatment.

Two additional human tumor cell lines (A431, human epidermoid carcinoma and MV4-11, AML) have been used to evaluate ABT-869 in a flank xenograft setting. In both cases, reduction in tumor size was observed after treatment with dose levels of ABT-869 equal to or less than used in the studies described above. As shown in Fig. 4E, treatment of mice with small A431 tumors (~0.25 g) resulted in suppression of tumor growth. Treatment of mice with large established tumors (~1.25 g, day 21) resulted in a decrease (~25%) in tumor size followed by prolonged tumor stasis. Removing treatment resulted in tumor growth at a rate similar to that in vehicle-treated mice (day 28). Resumption of treatment halted tumor growth and reduced tumor size (day 42).

Tumor regression (>50% reduction in tumor size) in response to treatment with ABT-869 was clearly evident

from results with a flank xenograft model using human myeloid leukemia cell line MV4-11 (Fig. 4F). Treatment of mice with established tumors (≈1 g) resulted in rapid tumor regression at doses ≥1.5 mg/kg bid. Larger tumors (>2 g) were also subject to regression upon treatment with ABT-869. Growth inhibition with subsequent reduction in tumor size was observed at doses as low as 0.5 mg/kg bid.

Orthotopic Tumor Growth Models

ABT-869 has been evaluated in an orthotopic setting with two breast carcinoma cell lines: MDA-231 (epithelial) and MDA-435LM (ductal). As monotherapy, ABT-869 exhibited efficacy in the orthotopic setting (Fig. 5A and B) comparable with that observed in the flank models described above. In combination, ABT-869 augmented the effects seen with paclitaxel in both of the orthotopic models. ABT-869 was also effective in a rat orthotopic glioma model. Administration of ABT-869 (1.5, 5, and 10 mg/kg bid) to rats bearing brain tumors derived from rat 9L cells resulted in dose-dependent inhibition of tumor growth (Fig. 5C). The efficacy at the highest dose (67% inhibition) was similar to that achieved in the breast orthotopic model and illustrates the effectiveness of ABT-869 in a nonmurine species.

In parallel studies with s.c. tumors derived from the MDA-231 breast carcinoma cell line immunohistologic examination was used to examine the effect of treatment with ABT-869 on tumor vascularization. Analysis of tumors resected after 3.5 days of treatment with ABT-869 (12.5 mg/kg bid) revealed a decrease in the density of CD31-positive vessels compared with vehicle treated (0.16% versus 0.49%, $P = 0.02$; Fig. 5D). The reduction in microvasculure density is consistent with an antiangiogenic mechanism of action of ABT-869.

Efficacious Drug Levels

In an effort to relate efficacy to drug exposure rather than dose, the concentration of ABT-869 was assayed in plasma samples obtained over a 12-hour period after the last dose at the completion of the efficacy studies. The relationship between efficacy and plasma concentration (C_{max}) or exposure (24-hour area under the curve or $AUC_{24\ hours}$) across a variety of tumor models is illustrated in Fig. 6. These results highlight the variability in sensitivity to treatment with ABT-869. Thus, for a given exposure (e.g., 2.7 μg·hour/mL), efficacy ranges from 100% (highly responsive, A431) to 75% (moderately responsive, HT1080) to 35% inhibition (relatively resistant, MDA-435). Thus, choosing a value for efficacious exposure, whether in terms of C_{max} or $AUC_{24\ hours}$, is by necessity model dependent. The moderately sensitive HT1080 fibrosarcoma model was selected as a representative, or benchmark, model for defining pharmacokinetic targets for robust tumor growth efficacy (75% inhibition). As shown in Fig. 6A, the target C_{max} and $AUC_{24\ hours}$ for ABT-869 are 0.4 μg/mL and 2.7 μg·hour/mL, respectively.

Terminal plasma drug concentration data presented in Fig. 6B indicate that continuous inhibition of the target RTKs is not required for activity. The dose from the illustrated study with the HT1080 model provided ABT-869

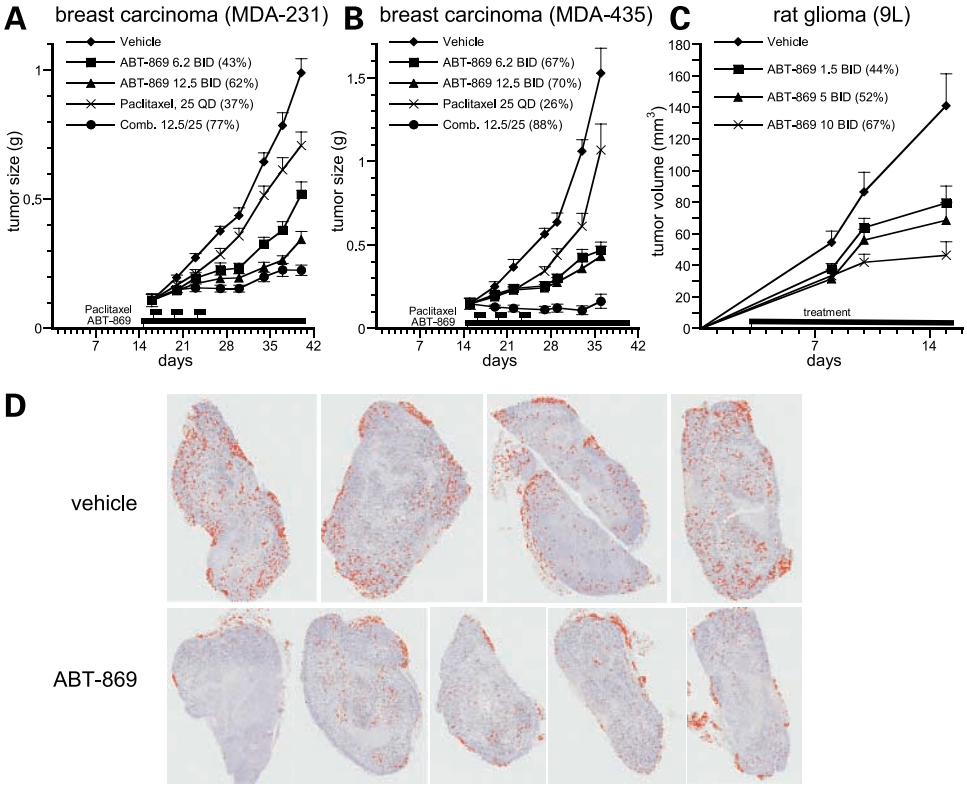

Figure 5. Activity in orthotopic tumor models. Effects of ABT-869 on the growth of human breast carcinoma MDA-231 (**A**) and MDA-435LM (**B**) cells implanted orthotopically in severe combined immunodeficient mice. Oral dosing of ABT-869 began on day 16 (10 per group). Paclitaxel was given i.p. on days 16, 20, and 24. **C,** rat glioma. Oral administration (bid) started on day 3 (12 per group). Dose (mg/kg bid) and percent inhibition of control (based on day 38 and 34, respectively). Significant differences ($P < 0.05$ versus control) in mean tumor volume were observed for all treatment groups by study end. **D,** CD31 staining of sections of MDA-231 tumors prepared from mice receiving either vehicle ($n = 4$) or ABT-869 ($n = 5$, 12.5 mg/kg bid, 3.5 d).

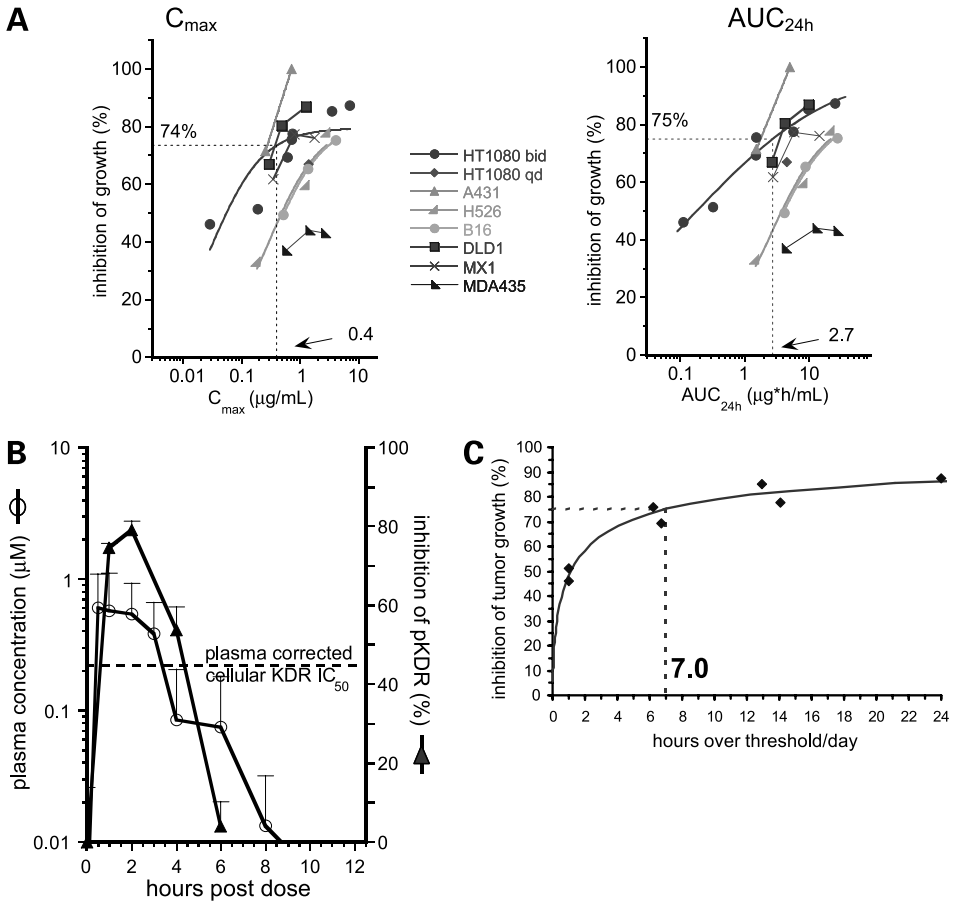

Figure 6. Plasma drug exposure associated with efficacy. **A,** relationship between C_{max} or AUC_{24h} and efficacy. **B,** drug plasma concentration and inhibition of KDR phosphorylation the HT1080 model. Plasma concentrations were determined at the end of an efficacy study with ABT-869 (5 mg/kg bid). *Points,* mean (n = 2); *bars,* SE. Inhibition of KDR phosphorylation was assessed in a satellite group at the indicated time after a single dose of ABT-869 (5 mg/kg bid). *Points,* mean (n = 3); *bars,* SE. **C,** relationship between duration of exposure and efficacy for the HT1080 tumor model.

plasma concentrations that exceed the IC_{50} for inhibition of cellular KDR in the presence of plasma (0.24 μmol/L) for only ~4 of the 12 hours in the bid dosing cycle, although this dose resulted in a 69% reduction in tumor growth. The extent of time above the plasma IC_{50} agrees well with the duration of >50% inhibition of a functional response to VEGF (uterine edema; Fig. 3C) and receptor phosphorylation (Fig. 6B).

As is shown in Fig. 6A for both C_{max} and $AUC_{24\ hours}$, splitting the total daily dose into two doses (bid: 77%) was statistically ($P < 0.01$) more effective than the same dose given once daily (qd, 67%). The observation that increasing dosing frequency at least maintains efficacy in the HT1080 model implies that longer but not necessarily complete coverage of the target may be preferred. Therefore, assessment of time over threshold is likely to be an important predictor of efficacy. The relationship between duration of exposure and efficacy of ABT-869 in the HT1080 model is illustrated in Fig. 6C. This relationship suggests that ABT-869 exposure exceeding threshold values for 7 of 24 hours is sufficient for robust (>75%) tumor growth inhibition.

Comparison with Other Tyrosine Kinase Inhibitors

To gain an understanding of the potential clinical merit of ABT-869, the inhibition profile of ABT-869 against a panel of kinases was compared with the profiles of five previously described inhibitors that have undergone clinical development (58–60). Hierarchical clustering of enzyme inhibition potency (Fig. 7A) reveals that ABT-869 provides complete coverage ($K_i \leq 10$ nmol/L) of the targeted kinases (VEGF and PDGF RTKs). By comparison, the relatively selective inhibitors PTK787 and BAY 43-9006 are only partially effective against the VEGF and PDGF family of kinases. AG013736, CHIR 258, and SU 11248 are active against most of the targeted kinases. However, these inhibitors exhibit more activity against nontargeted kinases than does ABT-869.

The *in vivo* activities of the reference kinase inhibitors were assessed in the VEGF-mediated uterine edema model. As is illustrated in Fig. 7B, ABT-869 is more potent than the other inhibitors in blocking VEGF-induced edema.

Discussion

ABT-869 is a novel, ATP-competitive inhibitor of VEGF and PDGF RTKs that lacks significant activity against representative cytosolic tyrosine kinases and serine/threonine kinases. The selectivity profile of ABT-869 differs from several previously described inhibitors (e.g., PTK787, ZD6474, CP-547,632, and AG013736) and antibodies (Avastin) that are more restricted to KDR and VEGF (58–60). Simultaneous inhibition by ABT-869 of the VEGF and PDGF RTKs, which mediate tumor progression by multiple mechanisms, may result in greater antitumor

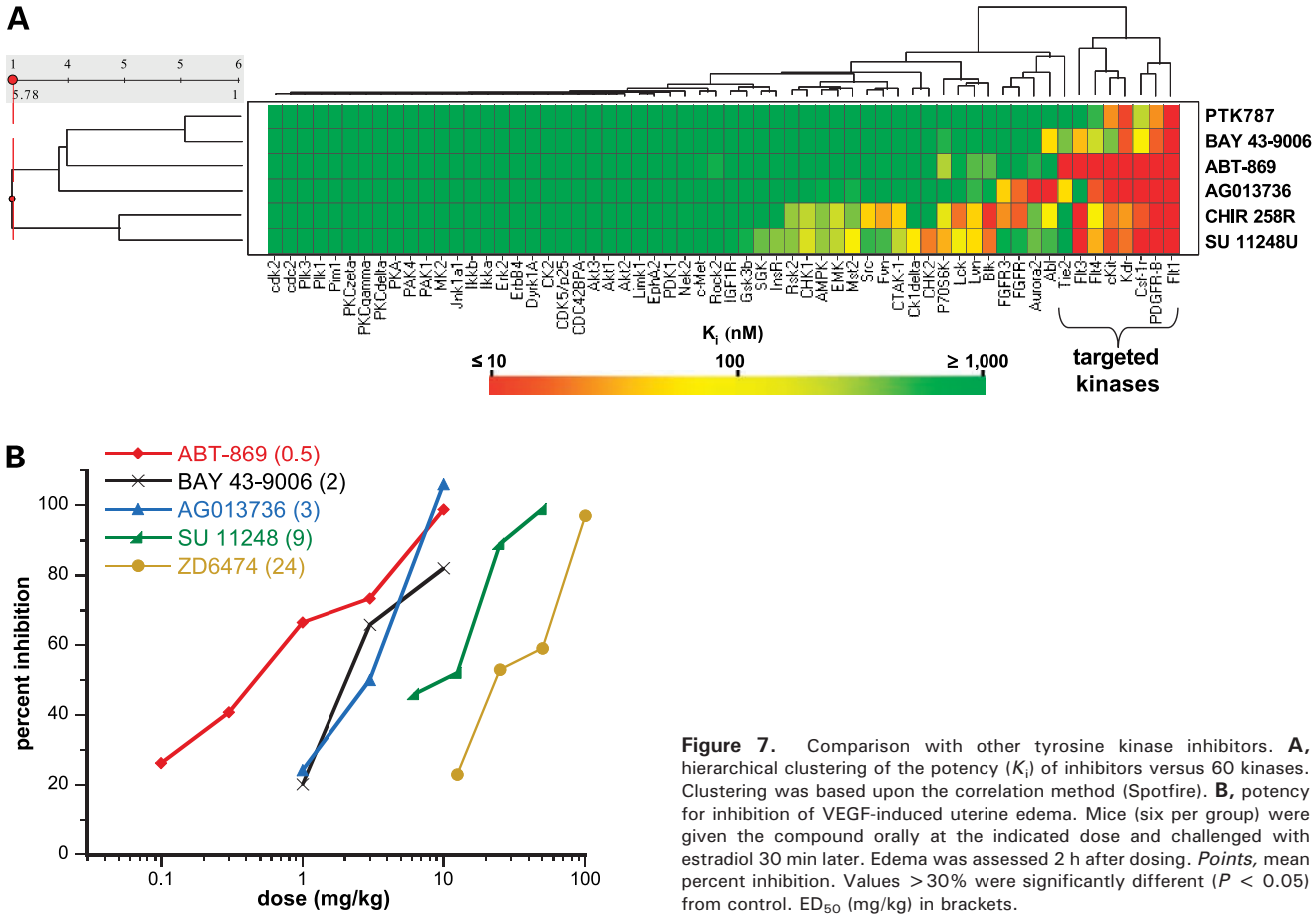

Figure 7. Comparison with other tyrosine kinase inhibitors. **A,** hierarchical clustering of the potency (K_i) of inhibitors versus 60 kinases. Clustering was based upon the correlation method (Spotfire). **B,** potency for inhibition of VEGF-induced uterine edema. Mice (six per group) were given the compound orally at the indicated dose and challenged with estradiol 30 min later. Edema was assessed 2 h after dosing. *Points,* mean percent inhibition. Values >30% were significantly different ($P < 0.05$) from control. ED_{50} (mg/kg) in brackets.

efficacy and provides the potential to treat a broader range of human cancers than more selective agents. The validity of a multitargeted approach is supported by recent reports of promising clinical results in two renal cell carcinoma studies with SU11248, a molecule that exhibits a similar VEGF and PDGF inhibitory profile to ABT-869. Partial responses were achieved in 40% of patients given SU11248 (61). However, toxicity, primarily grade 1 or 2 fatigue, diarrhea, and/or nausea, necessitates dosing holidays of 2 weeks in each 6-week cycle. These adverse effects may be a consequence of uninterrupted RTK inhibition due to the compound's 40-hour half-life (62, 63) or, alternatively, may reflect activity against off-target kinases exhibited by SU11248 and other kinase inhibitors (Fig. 7A).

Consistent with the putative mode of action defined with isolated enzyme preparations, ABT-869 exhibited potent activity (IC_{50}s = 2–30 nmol/L) for inhibiting KDR, PDGFR-β, KIT, and CSF-1R phosphorylation in intact cells. However, although effective against most members of the KDR and PDGF family of RTKs that were evaluated using intact cell assays, ABT-869 was only marginally active (IC_{50} = 3.5 μmol/L) in inhibiting phosphorylation of TIE2 in a cellular setting in spite of exhibiting submicromolar potency (170 nmol/L) in the isolated enzyme assay. Unlike the other cellular constructs used in these studies, the TIE2 construct relied on an autocrine loop for activation and may therefore not accurately reflect the sensitivity of a ligand-activated kinase to ABT-869. Further studies will be necessary to understand the basis of this discrepancy between TIE2 potency in the isolated enzyme and cellular settings.

Other examples of mechanism-based cellular activity include the inhibition of KDR-dependent proliferation of endothelial cells and the FLT3-dependent proliferation of MV4-11 leukemia cells. ABT-869 causes a decrease in the phosphorylation of both FLT3 and the downstream signaling protein signal transducers and activators of transcription 5 at the same concentrations in which inhibition of proliferation of MV4-11 cells is observed.[1] Interestingly, in contrast, inhibition of VEGF-induced proliferation of endothelial cells occurs at a concentration 10-fold lower than inhibition of KDR phosphorylation. This raises the possibility that additional kinases targeted by ABT-869 may play a role in VEGF signaling in endothelial cells. This interesting possibility notwithstanding, the *in vivo* potency for inhibiting KDR phosphorylation and a

[1] J. Li et al. ABT-869 a multi-targeted receptor tyrosine kinase inhibitor: inhibition of FLT3 phosphorylation and signaling in acute myeloid leukemia. Cancer Res, submitted for publication.

VEGF functional response (edema) are comparable, which further supports the mode of action of ABT-869 as inhibition of VEGF receptor activation. These observations do not preclude a contribution to efficacy due to inhibition of other growth factor receptors, particularly PDGFR-β, which plays an important role in maintaining tumor vasculature (64). Further studies will be necessary to assess the contribution of other target receptors to the activity of ABT-869. In any case, the potent and direct effects of ABT-869 on VEGF signaling suggest the possibility of observing mechanism-based responses early in the clinical development of ABT-869.

ABT-869 showed efficacy in a broad spectrum of xenograft tumor growth models, including human fibrosarcoma and breast, colon, and small cell lung carcinomas. ABT-869 has also been shown to be effective in an orthotopic model of prostate cancer in rat (data not shown). Although effective in all models tested, certain tumor types seemed more sensitive to treatment with ABT-869 than others. Treatment of mice bearing xenografts derived from epidermoid carcinoma or AML cells with ABT-869 resulted in a reduction in tumor size, whereas the small cell lung carcinoma model (H526) was somewhat less sensitive to treatment (60% inhibition of tumor growth, 5 mg/kg bid).

The antiangiogenic effects of ABT-869 presumably contribute to its antitumor efficacy, particularly in models that use highly vascular tumors, such as MX-1 and HT1080, that are known to express angiogenic factors (54, 55, 57). In that regard, immunohistochemical evidence showing a decrease in tumor vasculature as a result of treatment with ABT-869 was obtained in the breast carcinoma model. Nonetheless, the exquisite sensitivity to ABT-869 *in vivo* of other tumor cells, such as MV4-11-derived tumors, may be due, at least in part, to the potent antiproliferative activity of ABT-869 for tumor cells expressing mutated receptor kinases that are constitutively active (e.g., FLT3-ITD). Indeed, ABT-869 has been shown to inhibit FLT3 phosphorylation, increase apoptotic cells, and decrease proliferation of MV4-11 cells *in vivo*, supporting a direct effect of ABT-869 on these cells.[1] However, overexpression of wild-type target kinases that require ligand activation is not sufficient to confer high sensitivity because the H526 cells used in the small cell lung carcinoma model in the current studies (only moderately sensitive to ABT-869) are known to express high levels of the targeted kinase KIT (56). This suggests that ligand-independent activation is key to kinase-dependent tumor growth.

Based on plasma drug exposure data from the preclinical murine experiments, pharmacokinetic targets in the mouse were identified as $AUC_{24\ hours} \geq 2.7\ \mu g \cdot h/mL$ or plasma concentrations above the threshold value of 0.08 μg/mL for ≥7 hours. The duration of exposure required for antitumor efficacy agrees well with duration of inhibition achieved *in vivo* at the receptor and functional level (>50% for 3–4 hours/12-hour dosing period) and implies that continuous suppression of the target receptor is not necessary for robust antitumor activity. These results are in contrast to previous reports with kinase inhibitors, indicating that constant target suppression is necessary for antitumor efficacy (49). The close relationship between the kinetics for receptor inhibition *in vivo* and plasma concentration suggests that the receptor interaction with ABT-869 is readily reversible.

In summary, the preclinical characteristics of ABT-869 suggest that this molecule may offer distinct advantages in the realm of kinase inhibitors in cancer therapy. It is a multitargeted inhibitor that is focused on the VEGF and PDGF family of RTKs and lacks activity against off-target kinases. This profile, coupled with the ability to provide intermittent inhibition of target kinases and still maintain antitumor efficacy, may provide a unique clinical advantage by presenting an opportunity to avoid adverse reactions that are associated with long-term exposure to kinase inhibitors without relying on dosing holidays.

References

1. Hunter T. Signaling: 2000 and beyond. Cell 2000;100:113–27.
2. Manning G, Whyte DB, Martinez R, Hunter T, Sudarsanam S. The protein kinase complement of the human genome. Science 2002;298:1912–34.
3. Robinson DR, Wu YM, Lin SF. The protein tyrosine kinase family of the human genome. Oncogene 2000;19:5548–57.
4. Blume-Jensen P, Hunter T. Oncogenic kinase signalling. Nature 2001;411:355–65.
5. Hurwitz H, Fehrenbacher L, Novotny W, et al. Bevacizumab plus irinotecan, fluorouracil, and leucovorin for metastatic colorectal cancer. N Engl J Med 2004;350:2335–42.
6. Stirewalt DL, Radich JP. The role of FLT3 in haematopoietic malignancies. Nat Rev Cancer 2003;3:650–65.
7. Armstrong SA, Kung AL, Mabon ME, et al. Inhibition of FLT3 in MLL. Validation of a therapeutic target identified by gene expression based classification. Cancer Cell 2003;3:173–83.
8. Nakao M, Yokota S, Iwai T, et al. Internal tandem duplication of the flt3 gene found in acute myeloid leukemia. Leukemia 1996;10:1911–8.
9. Sawyers CL. Finding the next Gleevec: FLT3 targeted kinase inhibitor therapy for acute myeloid leukemia. Cancer Cell 2002;1:413–5.
10. Levis M, Small D. FLT3: ITDoes matter in leukemia. Leukemia 2003;17:1738–52.
11. Kottaridis PD, Gale RE, Linch DC. Flt3 mutations and leukaemia. Br J Dermatol 2003;122:523–38.
12. Lux ML, Rubin BP, Biase TL, et al. KIT extracellular and kinase domain mutations in gastrointestinal stromal tumors. Am J Pathol 2002;156:791–5.
13. Sommer G, Agosti V, Ehlers I, et al. Gastrointestinal stromal tumors in a mouse model by targeted mutation of the Kit receptor tyrosine kinase. Proc Natl Acad Sci U S A 2003;100:6706–11.
14. Akin C, Brockow K, D'Ambrosio C, et al. Effects of tyrosine kinase inhibitor STI571 on human mast cells bearing wild-type or mutated c-Kit. Exp Hematol 2003;31:686–92.
15. Yoshiji H, Harris SR, Thorgeirsson UP. Vascular endothelial growth factor is essential for initial but not continued *in vivo* growth of human breast carcinoma cells. Cancer Res 1997;57:3924–8.
16. Relf M, LeJeune S, Scott PA, et al. Expression of the angiogenic factors vascular endothelial cell growth factor, acidic and basic fibroblast growth factor, tumor growth factor beta-1, platelet-derived endothelial cell growth factor, placenta growth factor, and pleiotrophin in human primary breast cancer and its relation to angiogenesis. Cancer Res 1997;57:963–9.
17. Taylor AP, Osorio L, Craig R, et al. Tumor-specific regulation of angiogenic growth factors and their receptors during recovery from cytotoxic therapy. Clin Cancer Res 2002;8:1213–22.
18. Bergers G, Javaherian K, Lo KM, Folkman J, Hanahan D. Effects of angiogenesis inhibitors on multistage carcinogenesis in mice. Science 1999;284:808–12.

19. Viloria-Petit A, Crombet T, Jothy S, et al. Acquired resistance to the antitumor effect of epidermal growth factor receptor-blocking antibodies *in vivo*: a role for altered tumor angiogenesis. Cancer Res 2001;61:5090 – 101.

20. Cao R, Brakenhielm E, Pawliuk R, et al. Angiogenic synergism, vascular stability and improvement of hind-limb ischemia by a combination of PDGF-BB and FGF-2. Nat Med 2003;9:604 – 13.

21. Carmeliet P. Angiogenesis in health and disease. Nat Med 2003;9:653 – 60.

22. Benjamin LE, Golijanin D, Itin A, Pode D, Keshet E. Selective ablation of immature blood vessels in established human tumors follows vascular endothelial growth factor withdrawal. J Clin Invest 1999;103:159 – 65.

23. Richardson TP, Peters MC, Ennett AB, Mooney DJ. Polymeric system for dual growth factor delivery. Nat Biotechnol 2001;19:1029 – 34.

24. Bergers G, Song S, Meyer-Morse N, Bergsland E, Hanahan D. Benefits of targeting both pericytes and endothelial cells in the tumor vasculature with kinase inhibitors. J Clin Invest 2003;111:1287 – 95.

25. Gerber H-P, Ferrara N. The role of VEGF in normal and neoplastic hematopoiesis. J Mol Med 2003;81:20 – 31.

26. Cheng JD, Weiner LM. Tumors and their microenvironments: tilling the soil: commentary re: A. M. Scott et al., A phase I dose-escalation study of sibrotuzumab in patients with advanced or metastatic fibroblast activation protein-positive cancer. Clin Cancer Res 2003;9:1639 – 47. Clin Cancer Res 2003;9:1590 – 5.

27. Kunz-Schughart LA, Knuechel R. Tumor-associated fibroblasts (part I): active stromal participants in tumor development and progression? Histol Histopathol 2002;17:599 – 621.

28. Seljelid R, Jozefowski S, Sveinbjornsson B. Tumor stroma. Anticancer Res 1999;19:4809 – 22.

29. Camps JL, Chang SM, Hsu TC, et al. Fibroblast-mediated acceleration of human epithelial tumor growth *in vivo*. Proc Natl Acad Sci U S A 1990; 87:75 – 9.

30. Luttun A, Tjwa M, Moons L, et al. Revascularization of ischemic tissues by PlGF treatment, and inhibition of tumor angiogenesis, arthritis and atherosclerosis by anti-Flt1. Nat Med 2002;8:831 – 40.

31. Pei XH, Nakanishi Y, Takayama K, Bai F, Hara N. Granulocyte, granulocyte-macrophage, and macrophage colony-stimulating factors can stimulate the invasive capacity of human lung cancer cells. Br J Cancer 1999;79:40 – 6.

32. Yong LC. The mast cell: origin, morphology, distribution, and function. Exp Toxicol Pathol 1997;49:409 – 24.

33. Coussens LM, Raymond WW, Bergers G, et al. Inflammatory mast cells up-regulate angiogenesis during squamous epithelial carcinogenesis. Genes Dev 1999;13:1382 – 97.

34. Martinelli G, Piccaluga PP, Lo Coco F. FLT3 inhibition as tailored therapy for acute myeloid leukemia. Haematologica 2003;88:4 – 8.

35. Grundler R, Thiede C, Miething C, Steudel C, Peschel C, Duyster J. Sensitivity toward tyrosine kinase inhibitors varies between different activating mutations of the FLT3 receptor. Blood 2003;102:646 – 51.

36. Murata K, Kumagai H, Kawashima T, et al. Selective cytotoxic mechanism of GTP-14564, a novel tyrosine kinase inhibitor in leukemia cells expressing a constitutively active Fms-like tyrosine kinase 3 (FLT3). J Biol Chem 2003;278:32892 – 8.

37. Hyodo I, Doi T, Endo H, et al. Clinical significance of plasma vascular endothelial growth factor in gastrointestinal cancer. Eur J Cancer 1998;34:2041 – 5.

38. Obermair A, Kucera E, Mayerhofer K, et al. Vascular endothelial growth factor (VEGF) in human breast cancer: correlation with disease-free survival. Int J Cancer 1997;74:455 – 8.

39. Dai Y, Davidsen SK, Ericsson AM, Hartandi K, Ji Z, Michaelides MR. Indazole and benzisoxazole kinase inhibitors. U.S. Patent US 2004/ 0235892, Abbott Laboratories; 2003.

40. Freddo J, Hu-Lowe D, Pithavala YK, Steinfeldt H. Dosage forms and methods of treatment using VEGFR inhibitors. U.S. Patent US 2004/ 0224988, Agouron Pharmaceuticals, Inc.; 2004.

41. Lee SH, Lopes de Menezes D, Vora J, et al. *In vivo* target modulation and biological activity of CHIR-258, a multitargeted growth factor receptor kinase inhibitor, in colon cancer models. Clin Cancer Res 2005;11:3633 – 41.

42. Wilhelm SM, Carter C, Tang L, et al. BAY 43 – 9006 exhibits broad spectrum oral antitumor activity and targets the RAF/MEK/ERK pathway and receptor tyrosine kinases involved in tumor progression and angiogenesis. Cancer Res 2004;64:7099 – 109.

43. Sun L, Liang C, Shirazian S, et al. Discovery of 5-[5-fluoro-2-oxo-1,2-dihydroindol-(3*Z*)-ylidenemethyl]-2,4-dimethyl-1*H*-pyrrole-3-carboxylic acid (2-diethylaminoethyl)amide, a novel tyrosine kinase inhibitor targeting vascular endothelial and platelet-derived growth factor receptor tyrosine kinase. J Med Chem 2003;46:1116 – 9.

44. Wood JM, Bold G, Buchdunger E, et al. PTK787/ZK 222584, a novel and potent inhibitor of vascular endothelial growth factor receptor tyrosine kinases, impairs vascular endothelial growth factor-induced responses and tumor growth after oral administration. Cancer Res 2000;60:2178 – 89.

45. Kolb AJ, Kaplita PV, Hayes DJ, et al. Tyrosine kinase assays adapted to homogeneous time-resolved fluorescence. Drug Discovery Today 1998;3:333 – 42.

46. Luo Y, Smith RA, Guan R, et al. Pseudosubstrate peptides inhibit Akt and induce cell growth inhibition. Biochemistry 2004;43:1254 – 63.

47. Guo J, Marcotte P, McCall JO, et al. Inhibition of phosphorylation of the colony-stimulating factor-1 receptor (c-Fms) tyrosine kinase in transfected cells by ABT-869 and other tyrosine kinase inhibitors. Mol Cancer Ther 2006;5:1007 – 13.

48. Ma W, Tan J, Matsumoto H, et al. Adult tissue angiogenesis: evidence for negative regulation by estrogen in the uterus. Mol Endocrinol 2001;15:1983 – 92.

49. Sepp-Lorenzino L, Rands E, Mao X, et al. A novel orally bioavailable inhibitor of kinase insert domain-containing receptor induces antiangiogenic effects and prevents tumor growth *in vivo*. Cancer Res 2004;64:751 – 6.

50. Leung DW, Cachianes G, Kuang WJ, Goeddel DV, Ferrara N. Vascular endothelial growth factor is a secreted angiogenic mitogen. Science 1989;246:1306 – 9.

51. Yee KWH, O'Farrell A-M, Smolich BD, et al. SU5416 and SU5614 inhibit kinase activity of wild-type and mutant FLT3 receptor tyrosine kinase. Blood 2002;100:2941 – 9.

52. Sengupta K, Banerjee S, Saxena N, Banerjee SK. Estradiol-induced vascular endothelial growth factor-A expression in breast tumor cells is biphasic and regulated by estrogen receptor-alpha dependent pathway. Int J Oncol 2003;22:609 – 14.

53. Bold G, Frei J, Furet P, et al. CGP 79787D (PTK787/ZK222584), CGP 84738 NVP-AAC789, NVP-AAD777 and related 1-anilino-(4-pyridylmethyl)phthalazines as inhibitors of VEGF- and bFGF-induced angiogenesis. Drugs Future 2002;27:43 – 55.

54. Mukhopadhyay D, Tsiokas L, Sukhatme VP. High cell density induces vascular endothelial growth factor expression via protein tyrosine phosphorylation. Gene Expr 1998;7:53 – 60.

55. Kubota S, Mitsudomi T, Yamada Y. Invasive human fibrosarcoma DNA mediated induction of a 92 kDa gelatinase/type-IV collagenase leads to an invasive phenotype. Biochem Biophys Res Commun 1991;181:1539 – 47.

56. Abrams TJ, Lee LB, Murray LJ, Pryer NK, Cherrington JM. SU11248 inhibits KIT and platelet-derived growth factor receptor beta in preclinical models of human small cell lung cancer. Mol Cancer Ther 2003;2:471 – 8.

57. Marxsen JH, Schmitt O, Metzen E, Jelkmann W, Hellwig-Burgel T. Vascular endothelial growth factor gene expression in the human breast cancer cell line MX-1 is controlled by O2 availability *in vitro* and *in vivo*. Ann Anat 2001;183:243 – 9.

58. Supuran C, Scozzafava A. Protein tyrosine kinase inhibitors as anticancer agents. Expert Opinion on Therapeutic Patents 2004;14:35 – 53.

59. Rini BI, Small EJ. Biology and clinical development of vascular endothelial growth factor-targeted therapy in renal cell carcinoma. J Clin Oncol 2005;23:1028 – 43.

60. Mazitschek R, Giannis A. Inhibitors of angiogenesis and cancer-related receptor tyrosine kinases. Curr Opin Chem Biol 2004;8:432 – 41.

61. Motzer RJ, Rini BI, Michaelson MD, et al. Phase 2 trials of SU11248 show antitumor activity in second-line therapy for patients with metastatic renal cell carcinoma (RCC). 2005 ASCO Annual Meeting 2005;4508.

62. Sebolt-Leopold JS, Merriman R, Klohs W, et al. Highly selective kinase inhibitors: too much of a good thing [abstract PL0401]? Clin Cancer Res Suppl 2003;9:6267 – 8S.

63. Manning WC, Bello CL, Deprimo SE, et al. Pharmacokinetic and pharmacodynamic evaluation of SU11248 in a phase I clinical trial of patients (pts) with imatinib-resistant gastrointestinal stromal tumor (GIST) [abstract 768]. Proc Am Soc Clin Oncol 2003;22:192.

64. Inai T, Mancuso M, Hashizume H, et al. Inhibition of vascular endothelial growth factor (VEGF) signaling in cancer causes loss of endothelial fenestrations, regression of tumor vessels, and appearance of basement membrane ghosts. Am J Pathol 2004;165:35 – 52.

Molecular Cancer Therapeutics

Preclinical activity of ABT-869, a multitargeted receptor tyrosine kinase inhibitor

Daniel H. Albert, Paul Tapang, Terrance J. Magoc, et al.

Mol Cancer Ther 2006;5:995-1006.